

MR Imaging of Angiogenesis in Tumor Xenografts by $\alpha_v\beta_3$ - Targeted Magnetofluorescent Micellar Nanoprobes

C. W. Kessinger¹, C. Khemtong¹, O. Togao¹, M. Takahashi¹, and J. Gao¹

¹UT Southwestern Medical Center, Dallas, TX, United States

Introduction

One essential requirement for solid tumor growth is the ability to acquire an adequate blood supply; therefore, tumor vasculature is in a perpetual state of angiogenesis. Integrin $\alpha_v\beta_3$ is a well-established biomarker for angiogenesis with overexpression in tumor vasculature and low to no expression in resting endothelial cells.¹ Non-invasive assessment of tumor angiogenesis is important for early diagnosis of cancer as well as post-therapy assessment.^{2,3} Here we describe the use of $\alpha_v\beta_3$ targeted magnetofluorescent micelles to analyze angiogenesis in tumor xenografts and nanoprobe accumulation and kinetics by 3D magnetic resonance imaging (MRI) and T_2^* -weighted dynamic contrast enhancement MRI (DCE-MRI).

Experimental Methods

Methoxy poly(ethylene glycol)-b-poly(D,L lactic acid) (MeO-PEG-PLA) and maleimide-terminated PEG-PLA copolymers were synthesized via ring opening polymerization and used in combination with MeO-PEG-PLA copolymers conjugated with a fluorescent probe, tetramethylrhodamine (TMR, red fluorescence), PEG-PLA-TMR, for micelle formation. Superparamagnetic iron oxide (SPIO, dia. = 9 nm) nanoparticles were utilized. The FSPPM were conjugated with cRGD, a targeting ligand for $\alpha_v\beta_3$, or cRAD, non-targeted ligand, by maleimide chemistry. Cellular uptake and targeting specificity of cRGD-FSPPM was tested in SLK cells, which overexpress $\alpha_v\beta_3$ integrin and facilitate receptor-mediated endocytosis.⁴

For in vivo studies, A549 non-small cell lung cancer cells, were injected subcutaneously into the flank of athymic nude mice. Before injection, 3D MR images were collected. To analyze the kinetics of cRGD-FSPPM accumulation, T_2^* -weighted DCE-MRI was performed with a temporal resolution of 1.3s for 65 min where then taken during the injection of FSPPM (6mg/kg Fe). Images were divided by a mean pre-injection image (averaged from the first 30 sec of the DCE-MRI sequence, before injection). After DCE-MRI, post-injection (4hr) 3D MRI was performed to analyze spatial localization of the FSPPM. ImageJ, ITK-Snap and OsiriX programs were used to analyze data. The presence of FSPPM was validated by Prussian blue staining and immunofluorescence staining of sectioned tumor tissue. For pharmacokinetic studies, plasma was collected and analyzed for iron content (SPIO) by atomic absorption and radioactivity, from a tritium labeled PEG-PLA. MRI parameters for 2D or 3D gradient echo sequences. 2D: TR/TE= 10/3 ms, flip angle = 45°, NA=1, FOV: 40mm x 40mm, matrix=128 x 128, Scan Time=1.3 s. 3D: TR/TE=20/3 ms, flip angle=45°, NA=8, FOV=35 x 17.5 x 35 mm, matrix= 192 x 96 x 192, Scan Time = 50 min.

Results and Discussion

In vivo MR specificity of cRGD- and cRAD-FSPPM in mice bearing A549 tumor xenografts was analyzed. Pre- and post-injection images showed a greater darkening in tumor tissue in cRGD-FSPPM treated animals. 3D reconstruction of the tumor tissue was overlaid with the areas of darkening, due to FSPPM accumulation (Fig.1B). The distribution of the cRGD-FSPPM showed a branched network of darkening throughout the tumor, whereas cRAD-FSPPM treated tumors showed accumulation in the periphery of the tumor. Immunofluorescence and Prussian blue staining showed targeting of $\alpha_v\beta_3$ integrin by co-localization with cRGD-FSPPM fluorescence. Baseline images (0-30 s) before FSPPM injection showed constant image signal intensity. After FSPPM injection, blood vessels showed a decrease in SI and similar kinetic profiles in cRGD- and cRAD-FSPPM treated mice (red and blue lines, respectively). However, tumor hot-spots showed considerably different profiles between targeted (green) and non-targeted (pink) FSPPM-treated animals (Fig.1C). A sustained significant decrease of signal intensity was observed with cRGD-encoded SPPM, whereas the kinetic data from cRAD-FSPPM followed that from the major blood vessels. Muscle tissue showed significantly smaller initial decrease in SI and then a return to baseline over the one-hour imaging period (brown, Fig.1C). Pharmacokinetics of the FSPPM validated the clearance of the FSPPM from the blood, corroborating the kinetic profiles seen in the blood vessels in the DCE-MRI data. Similar pharmacokinetic profiles of the plasma for SPIO and polymer verified the integrity of the FSPPM in the blood (Fig. 1D), which is further supported by the SPIO-clustered micelle structure by TEM analysis (Fig. 1D, inset).

Conclusion

The $\alpha_v\beta_3$ -specific FSPPM nanoprobes showed increase in tumor accumulation compared to non-specific cRAD-FSPPM nanoprobes. The combination of 3D visualization and DCE-MRI with a cancer-targeted, magnetofluorescent FSPPM may offer new insights on molecular imaging of tumor angiogenesis and the targeting of nanoparticles in vivo.

References 1. Brooks PC, et al. Science 1994. 2. Weissleder R, et al. Nature 2008. 3. Cai W, et al. J Nucl Med 2008. 4. Nasongkla N, et al. Nano Lett 2006.

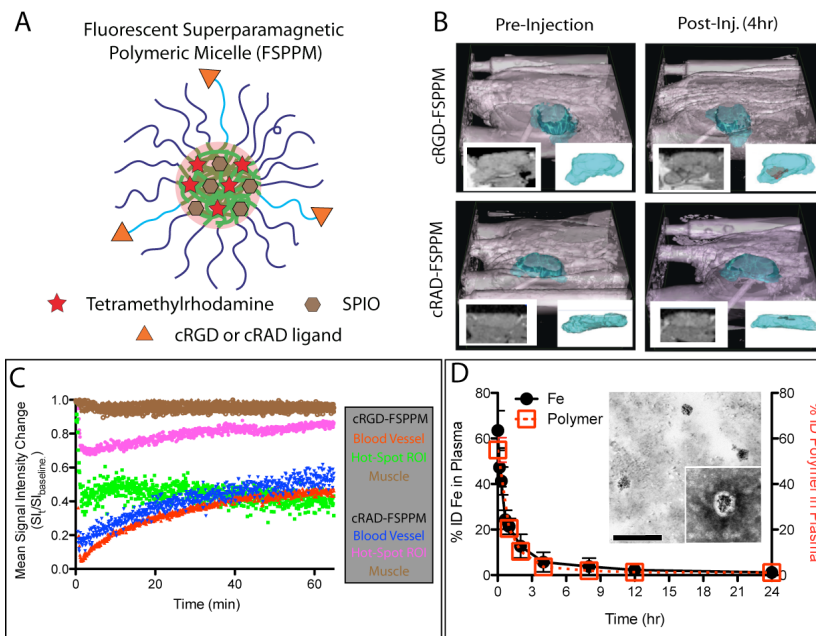


Figure 1. In vivo MRI of angiogenesis using cRGD-FSPPM nanoprobes. (A) Scheme of FSPPM. (B) 3D images of 3D data sets show mouse (purple), tumor (teal) and areas of darkening (red) overlaid. Insets-MRI image of tumor (left) and tumor (right). (C) DCE-MRI kinetic profiles of regions-of-interest (ROI) over 65 minutes. (D) Pharmacokinetics of FSPPM by iron and radiolabeled polymer in the plasma. Inset-TEM of micelles in the plasma at 1 hour. Scale bar = 200nm.